The Astrophysical Journal, 648:L33–L37, 2006 September 1

THE X-RAY SYNCHROTRON EMISSION OF RCW 86 AND THE IMPLICATIONS FOR ITS AGE

Jacco Vink,[1,2] Johan Bleeker,[1,2] Kurt van der Heyden,[3] Andrei Bykov,[4] Aya Bamba,[5] and Ryo Yamazaki[6]

Received 2006 June 13; accepted 2006 July 13; published 2006 August 14

ABSTRACT

We report X-ray imaging spectroscopy observations of the northeastern shell of the supernova remnant RCW 86 using *Chandra* and *XMM-Newton*. Along this part of the shell, the dominant X-ray radiation mechanism changes from thermal to synchrotron emission. We argue that both the presence of X-ray synchrotron radiation and the width of the synchrotron-emitting region suggest a locally higher shock velocity of $V_s \approx 2700$ km s^{-1} and a magnetic field of $B \approx 24 \pm 5$ μG. Moreover, we also show that a simple power-law cosmic-ray electron spectrum with an exponential cutoff cannot explain the broadband synchrotron emission. Instead, a concave electron spectrum is needed, as predicted by nonlinear shock acceleration models. Finally, we show that the derived shock velocity strengthens the case that RCW 86 is the remnant of SN 185.

Subject headings: shock waves — supernova remnants — X-rays: individual (RCW 86)

1. INTRODUCTION

Since the discovery of X-ray synchrotron radiation from SN 1006 (Koyama et al. 1995), it has been found that most young, shell-type supernova remnants (SNRs) emit X-ray synchrotron radiation (see Vink 2006 for a review). For the youngest SNRs, Cas A, Kepler (SN 1604), and Tycho (SN 1572), this radiation is confined to a narrow region close to the shock front. This does not seem to be the case for somewhat older, but physically much larger objects like RCW 86, G266.2−1.2 (Slane et al. 2001), and G347.3−0.5 (Cassam-Chenaï et al. 2004). The X-ray emission from the latter two SNRs does in fact reveal only synchrotron radiation, and both SNRs have been detected in TeV gamma rays (Aharonian et al. 2005, 2004).

It has been shown that the thickness of the X-ray synchrotron-emitting region is directly related to the postshock magnetic field strength (e.g., Vink & Laming 2003). The relatively strong fields found are probably a result of magnetic field amplification by cosmic-ray streaming (e.g., Bell 2004; Bykov & Toptygin 2005). The presence of X-ray synchrotron radiation is in itself an indication of efficient acceleration, and if the cutoff energy of the photon spectrum is determined by synchrotron losses, it is independent of the magnetic field strength but scales with shock velocity, as proportional to V_s^2 (Aharonian & Atoyan 1999).

Here we report on the analysis of *Chandra* and *XMM-Newton* data of the northeastern (NE) part of RCW 86 (G315.4−2.1). RCW 86 is an interesting SNR. The nonthermal X-ray–emitting regions are broader than those of the historical SNRs, and they are not confined to the forward shock region, possibly as a result of projection effects (Vink et al. 1997). In that respect, RCW 86 resembles G266.2−1.2 and G347.3−0.5. However, unlike those SNRs, RCW 86 also emits noticeable thermal X-ray emission. This allows for the determination of plasma properties, which can help us determine the conditions that may potentially lead to X-ray synchrotron emission in older SNRs. In particular, the NE part seems best suited for that purpose, since the X-ray synchrotron radiation is confined to the region directly behind the shock front, and, as a result, the geometry of the emitting region is easier to asses.

2. OBSERVATIONS AND ANALYSIS

The NE part of RCW 86 was observed by *Chandra* and *XMM-Newton* for their joint program. The *Chandra* observation (ID 500436) has a net exposure time of 72.6 ks and was made on 2004 June 6. The *XMM-Newton* observation (ID 0208000101) was made on 2004 January 26 with an exposure time of 60 ks. Both *Chandra* and *XMM-Newton* observed other parts of RCW 86 before (e.g., Rho et al. 2002). Here we present *Chandra* imaging of the NE part of RCW 86 (Fig. 1 [Plate 1]), but for spectroscopy we focus on the spectra obtained with the European Photon Imaging Camera metal oxide semiconductor (EPIC MOS; Turner et al. 2001) on *XMM-Newton*, since it offers us the best spectral resolution. For comparison, we also present an analysis of EPIC-MOS data of an observation of the northern part of RCW 86 (ObsID 0110011401, 18 ks). Moreover, we used all six observations of RCW 86 by *XMM-Newton* to produce the X-ray map shown in Figure 2. It also shows the spectral extraction regions. Background spectra were taken from regions outside the SNR. The data reduction was done with the standard software packages, CIAO 3.0 for *Chandra* and SAS 6.5.0 for *XMM-Newton*.

The spectrum from the region labeled "NE" (Fig. 3) shows an absence of bright line features. This is usually taken as a sign for synchrotron emission (Bamba et al. 2000; Borkowski et al. 2001; Rho et al. 2002), but for RCW 86 it has been argued by some of us in the past that nonthermal bremsstrahlung may be a viable mechanism as well (Vink et al. 1997). One of the reasons was the detection of Fe K emission at 6.4 keV in the southwest coinciding with the hard X-ray continuum. This interpretation was disputed by Rho et al. (2002), based on energetic grounds. Here we concur with that view. In fact, the *XMM-Newton* and *Chandra* spectra of the NE region do not show any evidence of Fe K emission, providing additional evidence for an X-ray synchrotron interpretation.

Figure 1 shows that along the shell, the X-ray emission changes from thermal radiation to predominantly synchrotron radiation. Unlike in other parts of RCW 86, it is unambiguous that in the NE, the nonthermal emission starts at the shock front. Surprisingly, the radio map shows that in the NE, the X-ray synchrotron ra-

[1] Astronomical Institute, University Utrecht, P.O. Box 80000, 3508TA Utrecht, Netherlands; j.vink@astro.uu.nl.
[2] SRON Netherlands Institute for Space Research, Sorbonnelaan 2, 3584CA, Utrecht, Netherlands.
[3] South African Astronomical Observatory P.O. Box 9, Observatory 7935, South Africa.
[4] Ioffe Physico-Technical Institute, Politekhnicheskaya 26, 194021 St. Petersburg, Russia.
[5] RIKEN, 2-1 Hirosawa, Wako, Saitama 351-0198, Japan.
[6] Department of Physics, Hiroshima University, Higa-shi, Hiroshima 739-8526, Japan.

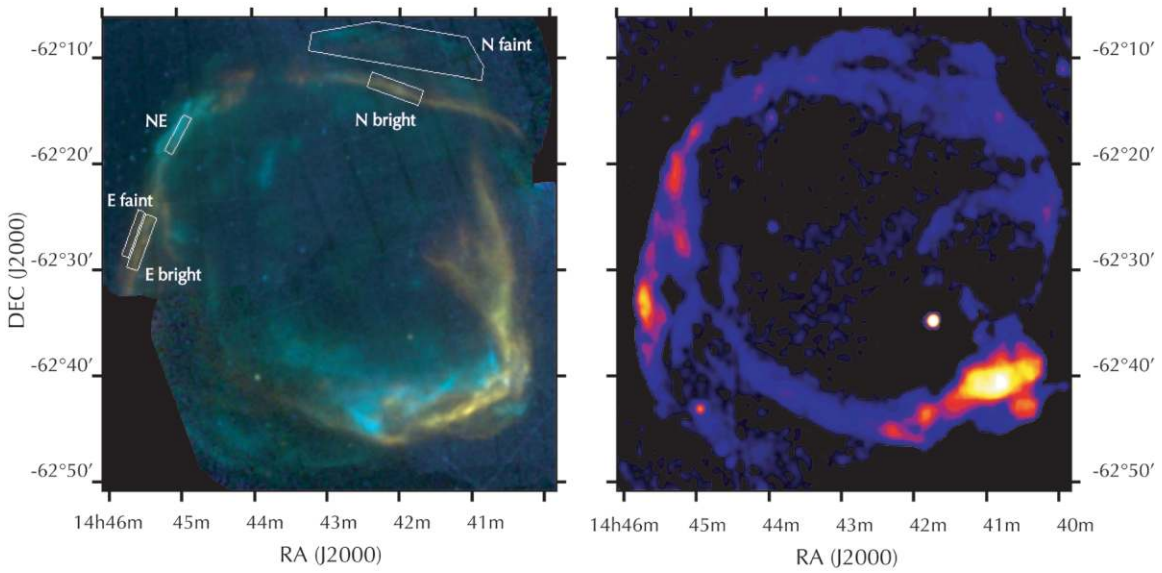

FIG. 2.—*Left*: *XMM-Newton* EPIC (MOS/PN) mosaic of RCW 86, with a color coding similar to Fig. 1, using a square root brightness scaling. Spectral extraction regions are overlaid. *Right*: Archival Molonglo Observatory Synthesis Telescope (MOST) 0.84 GHz radio map (Whiteoak & Green 1996; Dickel et al. 2001).

diation is not associated with bright radio emission but instead with relatively weak radio emission. In order to better determine the plasma conditions of the X-ray synchrotron-emitting regions, we do not present here the spectrum extracted from the whole X-ray synchrotron-emitting region but rather from a smaller region, labeled "NE" in Figure 2, which shows more traces of thermal emission. Apart from the NE shell, we also analyzed a faint region outside the main shell ("N faint"), which shows up better in radio than in X-ray.

We fitted the EPIC-MOS spectra using the spectral analysis software SPEX (Kaastra & Mewe 2000). The spectra are reasonably well described by a combination of two nonequilibrium ionization (NEI) models or, for the X-ray synchrotron-dominated regions, by one NEI model and a power-law spectrum (Table 1). The spectral fits indicate extreme departures from collisional equilibration, even compared to other young SNRs, except for SN 1006 (Vink et al. 2003). Although the fit quality is not always satisfactory, both the fitted models and the raw spectra itself (Fig. 3) show that the fainter the thermal emission, the lower the ionization degree. This can be judged from the increase of O VIII with respect to the O VII emission and presence of Fe L emission from the brighter parts. There is also a hint that the X-ray synchrotron-emitting regions contain hotter plasma, and they are characterized by lower ionization parameters ($n_e t$). However, we caution that, since most of the continuum is nonthermal, the temperature is solely determined by line ratios, making it more sensitive to potential errors in the atomic data. This may also explain the peculiarity that whenever a second thermal component was fitted, its best $n_e t$ value was much higher than the principal component. The second component improved, in particular, the fit between 1 and 1.2 keV, dominated by $n = 3 \rightarrow 1$ Ne IX line emission.

3. DISCUSSION

A recent development in the interpretation of X-ray synchrotron radiation is that the width of the region can be used

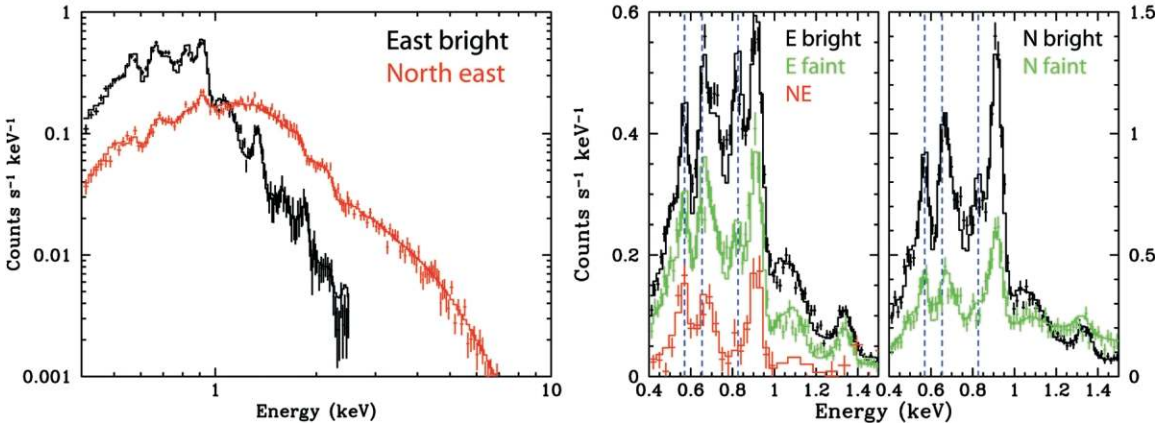

FIG. 3.—*XMM-Newton* EPIC-MOS spectra from the regions labeled in Fig. 2. *Left*: Logarithmic plots of a thermal and a nonthermal spectrum. *Right*: Comparison of the line emission from various regions. From the northeastern spectrum (*in red, left panel*), the best-fit power-law model has been subtracted in order to emphasize the thermal emission. Dashed lines indicate (*from left to right*) the energies of O VII Heα, O VIII Lyα, and Fe XVIII line emission.

TABLE 1
BEST-FIT MODELS FOR THE *XMM-NEWTON* MOS1 AND 2 SPECTRA

Parameter	NE	E-bright	E-faint	N-bright	N-faint
EM_1 (10^{53} cm^{-3} kpc^{-2})	12.6 ± 1.9	311 ± 45	70.6 ± 8.0	219 ± 48	69.5
kT_{e1} (keV)	6.7 ± 2.6	0.57 ± 0.05	0.93 ± 0.07	0.96 ± 0.13	6.3 ± 1.6
$n_e t_1$ (10^9 cm^{-3} s)	2.25 ± 0.15	6.7 ± 0.6	5.67 ± 0.03	4.0 ± 0.3	2.27 ± 0.12
EM_2 (10^{53} cm^{-3} kpc^{-2})	…	43.8 ± 5.3	…	40.9 ± 5.6	…
kT_{e2} (keV)	…	3.0 ± 0.3	…	3.2 ± 0.6	…
$n_e t_2$ (10^9 cm^{-3} s)	…	17.0 ± 0.5	…	19.7 ± 0.9	…
O	1	0.56 ± 0.06		0.68 ± 0.09	1
Ne	1	0.59 ± 0.04		0.72 ± 0.07	1
Mg	1	0.44 ± 0.04		0.39 ± 0.05	1
Si	1	0.27 ± 0.04		0.38 ± 0.07	1
Fe	1	0.64 ± 0.07		0.79 ± 0.14	1
PL norm. (10^{-3} s^{-1} keV^{-1} cm^{-2})	1.22 ± 0.03	…	…	…	1.8 ± 0.1
Γ	2.82 ± 0.04	…	…	…	3.5 ± 0.2
N_H (10^{21} cm^{-2})	4.1 ± 0.1	3.6 ± 0.2		3.6 ± 0.2	3.9 ± 0.2
C-statistics/dof	190.6/169	(302 + 260)/230		182/85	242/103

NOTE.—The models consist of either one or two NEI components, or of an NEI component with an additional power-law component. Abundances are given with respect to the solar abundances of Anders & Grevesse (1989). An entry "1" means the abundance as fixed to the solar value. Entries covering two columns were obtained by fitting two spectra simultaneously and forcing the parameters to be identical. The emission measure, EM, is defined as $\int n_e n_H \, dV/d^2$. The power-law (PL) normalization is given at 1 keV. All errors are 1 σ errors ($\Delta\chi^2 = 1$).

to estimate the downstream magnetic field. However, different groups have used, at face value, different methods for estimating the magnetic field: Vink & Laming (2003) assumed that the width, l, of the X-ray synchrotron-emitting region is determined by a combination of plasma velocity relative to the shock front, u, and the synchrotron loss time $\tau_{\rm loss} = 637/B^2E$, i.e., $l_{\rm adv} = u\tau_{\rm loss}$, with E the particle energy in units of ergs and B the magnetic field strength in units of gauss. The other method assumes that the width corresponds to the diffusion length scale (Bamba et al. 2005; Völk et al. 2005), given by $l_{\rm diff} = D/u$, with $D = cE/3eB$ the diffusion coefficient. In essence, $l_{\rm diff}$ is the length scale at which advection starts to dominate over diffusion as the means of transporting particles. Both methods give a combination of E and B, which can be solved by using the fact that the observed photon energies peak around $\epsilon = 7.4BE^2$ keV. Both methods rely on different assumptions. First of all, for standard shocks, $u = V_s/4$, but for very efficient shock acceleration, the compression factor may be stronger than a factor 4. Second, the diffusion length method assumes $D = cE/3eB$, which is the smallest diffusion coefficient possible, as the particle mean free path is then equal to the gyroradius (the "Bohm limit").

It turns out that with both methods, very similar magnetic field estimates are obtained (Ballet 2006; Vink 2006). As shown by Vink (2006), this is to be expected if one observes the X-ray synchrotron spectrum near the spectral cutoff energies: The acceleration time for particles according to the first-order Fermi acceleration theory is, within a factor of order 1, $\tau_{\rm acc} \approx D/u^2$ (Malkov & Drury 2001). For electrons, the acceleration is limited by synchrotron losses. So there is only a net acceleration if $\tau_{\rm acc} < \tau_{\rm loss}$, and the maximum energy is reached when $\tau_{\rm acc} \approx \tau_{\rm loss}$ (Reynolds 1998). Therefore,

$$\tau_{\rm acc} \approx \tau_{\rm loss} \Longleftrightarrow D/u \approx u\tau_{\rm loss} \Longleftrightarrow l_{\rm diff} \approx l_{\rm adv}. \quad (1)$$

In other words, $l_{\rm diff} \approx l_{\rm adv}$ is the geometrical equivalent of $\tau_{\rm loss} \approx \tau_{\rm acc}$. Note that the *observational* fact that the diffusion length scale and advection length scale methods give similar results is a justification for the assumption that the diffusion coefficient is close to the Bohm limit and that the shock compression ratio is close to the standard value of 4 (Vink 2006).

The *Chandra* image reveals a width of the X-ray synchrotron shell of ~100″, corresponding to 3.7×10^{18} cm for a distance of $d = 2.5$ kpc (Westerlund 1969; Rosado et al. 1994). Fitting a projected shell model, we estimate a physical width of 1.7×10^{18} cm. In addition, we apply a factor 0.6, because the actual width is a convolution of advection and diffusion processes (i.e., we set $l_{\rm diff} = l_{\rm adv}$ in eq. [1] of Berezhko & Völk 2004), so $l_{\rm adv} = 1.0 \times 10^{18}$ cm. Assuming that the shock velocity is $V_s = 600$ km s^{-1} (Ghavamian et al. 2001) gives inconsistent results for the two methods: $B \sim 90$ μG employing the diffusion length method, and 6 μG assuming the advection length method.

However, if we no longer assume a shock velocity of 600 km s^{-1}, which after all was based on optical observations of a different part of RCW 86 from which no X-ray synchrotron radiation is emitted, we can use the condition that $l_{\rm adv} = l_{\rm diff}$ in order to estimate V_s and B, using an observed photon energy of $\epsilon \approx 1$ keV. We found that B can be directly estimated from the diffusion/advection length alone, whereas the plasma velocity only depends on the photon energy:

$$B \approx \left(\frac{c}{3e}\right)^{1/3} l_{\rm adv}^{-2/3} = 24 \left(\frac{l_{\rm adv}}{1.0 \times 10^{18}\ {\rm cm}}\right)^{-2/3} \ \mu{\rm G}, \quad (2)$$

$$V_s = u\chi \approx \chi \sqrt{\frac{\epsilon}{7.4\ {\rm keV}} \frac{c}{3e \times 637}}$$

$$= 2650 \left(\frac{\chi}{4}\right) \sqrt{\frac{\epsilon}{1\ {\rm keV}}}\ {\rm km\ s^{-1}}, \quad (3)$$

where χ is the shock compression factor. Equation (3) was previously reported by Aharonian & Atoyan (1999). To get more accurate estimations, one has to solve the model-dependent kinetic equations for the particle distribution. For the moment, we estimate the error in the physical width due to distance uncertainties and projection effects to be ~30%, resulting in an error in B of ~5 μG. The downstream magnetic field therefore appears to be lower than for other SNRs (Vink 2006). There is some uncertainty in the actual cutoff energy of the synchrotron spectrum (see below), but uncertainties about the assumptions—

larger compression ratio, less efficient diffusion—make equation (3) effectively a lower limit.

One may wonder why the shock velocity in some regions may be so much higher, and why it has not resulted in a more distorted shell. Here the thermal spectra help us to answer this question. For all fitted regions, the $n_e t$ value of the primary component is low, being $n_e t = 6.7 \times 10^9$ cm^{-3} s even for the brightest region. From the size of our extraction box, we estimate that the emitting volume is $V = 10^{56}$–10^{57} cm^3; together with the emission measure this implies an electron density of $n_e = 0.5$–1.6 cm^{-3}. If we use this to estimate how long ago the plasma was shock-heated, we find $t \lesssim 425$ yr. This is surprisingly short for a large SNR such as RCW 86. In such a time, the difference in radius between regions with low and high shock velocity would be ~0.9 pc on an average shock radius of 16 pc. The short interaction time supports the idea that RCW 86 is a SNR expanding in a windblown bubble (Vink et al. 1997). Such SNRs expand rapidly for a long time, but the shock velocity drops rather suddenly as soon as the shock starts interacting with the surrounding shell that was swept up by the progenitor's stellar wind (e.g., Dwarkadas 2005). This suggests that in RCW 86, the shock has reached in some regions the dense shell around the bubble some 400 years ago, after which it rapidly decelerated. In other regions, the shock velocity is still high, but, due to the low density, the thermal X-ray emission is weak. This explains the coexistence of relatively weak radio synchrotron emission with conspicuous X-ray synchrotron emission: due to the lower density, fewer electrons are accelerated, but because of the high shock velocity, they can be accelerated to higher energies.

Interestingly, the X-ray synchrotron radiation is relatively bright, with respect to the radio emission, because we find that the simplest broadband synchrotron model, i.e., synchrotron radiation from a power-law electron spectrum with an exponential cutoff, does not fit the data (Fig. 4). It can explain the X-ray flux but not the spectral slope. Instead, the electron spectrum needs to be concave, as predicted by nonlinear shock acceleration models. However, we cannot determine whether the electron power-law index bends toward -2, predicted for an overall shock compression ratio of 4, or toward -1.5, predicted for strongly cosmic-ray–modified shocks (Berezhko & Ellison 1999).

The NE region of RCW 86 has properties resembling those of the TeV-emitting SNRs G347.3−0.5 and G266.2−1.2: weak radio emission, and X-ray emission (almost) entirely consisting

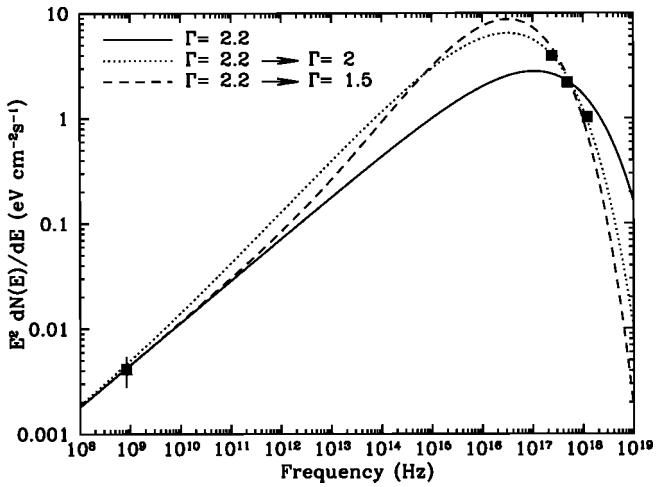

FIG. 4.—Broadband (νF_ν) spectrum of the NE region, with the 847 MHz flux density based on archival MOST data. The models consist of synchrotron radiation from a power law and concavely shaped electron energy distributions with exponential cutoffs at high energies, convolved with the synchrotron emission function (Ginzburg & Syrovatski 1965). The radio spectral index is fixed to $\alpha = -0.6$ (Caswell et al. 1975).

of synchrotron radiation. For RCW 86, the (weak) thermal X-ray emission indicates that these properties are due to a low density combined with a relatively high shock velocity. We speculate that for G347.3−0.5 and G266.2−1.2, the shock also moves through a low-density region, e.g., a stellar wind bubble, and the shock velocity is similarly high. RCW 86 may be different in that some parts of the shock have reached the shell. Inside the bubble, the shock evolution can be approximated by the Sedov self-similar model, but this breaks down as soon as the shell is reached. Finally, assuming a Sedov evolution and using the apparent radius of 22′, the age of the remnant is estimated to be $t = 2r/5V_s \approx 2250(V_s/2700 \text{ km s}^{-1})$ yr. This would put the explosion date of RCW 86 closer to AD 185, the year a putative supernova was observed in China (Stephenson & Green 2002). A shock velocity of ~600 km s^{-1} would be more consistent with a 10,000 year old SNR. Our results, therefore, strengthen the case that the event recorded by Chinese astronomers was indeed a supernova and that RCW 86 is its remnant.

J. V. is supported by a Vidi grant from the Netherlands Organisation for Scientific Research (NWO).

REFERENCES

Aharonian, F. A., & Atoyan, A. M. 1999, A&A, 351, 330
Aharonian, F. A., et al. 2004, Nature, 432, 75
———. 2005, A&A, 437, L7
Anders, E., & Grevesse, N. 1989, Geochim. Cosmochim. Acta, 53, 197
Ballet, J. 2006, Adv. Space Res., 37, 1902
Bamba, A., Koyama, K., & Tomida, H. 2000, PASJ, 52, 1157
Bamba, A., Yamazaki, R., Yoshida, T., Terasawa, T., & Koyama, K. 2005, ApJ, 621, 793
Bell, A. R. 2004, MNRAS, 353, 550
Berezhko, E. G., & Ellison, D. C. 1999, ApJ, 526, 385
Berezhko, E. G., & Völk, H. J. 2004, A&A, 419, L27
Borkowski, K. J., Rho, J., Reynolds, S. P., & Dyer, K. K. 2001, ApJ, 550, 334
Bykov, A. M., & Toptygin, I. N. 2005, Astron. Lett., 31, 748
Cassam-Chenaï, G., et al. 2004, A&A, 427, 199
Caswell, J. L., Clark, D. H., & Crawford, D. F. 1975, Australian J. Phys. Astrophs. Suppl., 39
Dickel, J. R., Strom, R. G., & Milne, D. K. 2001, ApJ, 546, 447
Dwarkadas, V. V. 2005, ApJ, 630, 892
Ghavamian, P., Raymond, J., Smith, R. C., & Hartigan, P. 2001, ApJ, 547, 995
Ginzburg, V. L., & Syrovatski, S. I. 1965, ARA&A, 3, 297
Kaastra, J. S., & Mewe, R. 2000, in Atomic Data Needs for X-Ray Astronomy, ed. M. A. Bautista, T. R. Kallman, & A. K. Pradhan (Greenbelt: NASA), 161
Koyama, K., et al. 1995, Nature, 378, 255
Malkov, M. A., & Drury, L. 2001, Rep. Prog. Phys., 64, 429
Reynolds, S. P. 1998, ApJ, 493, 375
Rho, J., Dyer, K. K., Borkowski, K. J., & Reynolds, S. P. 2002, ApJ, 581, 1116
Rosado, M., Le Coarer, E., & Georgelin, Y. P. 1994, A&A, 286, 231
Slane, P., et al. 2001, ApJ, 548, 814
Stephenson, F. R., & Green, D. A. 2002, Historical Supernovae and Their Remnants (Oxford: Clarendon)
Turner, M. J. L., et al. 2001, A&A, 365, L27
Völk, H. J., Berezhko, E. G., & Ksenofontov, L. T. 2005, A&A, 433, 229
Vink, J. 2006, in The X-Ray Universe 2005, Vol. 1, ed. A. Wilson (ESA SP-604; Noordwijk: ESA/ESTEC), 319
Vink, J., Kaastra, J. S., & Bleeker, J. A. M. 1997, A&A, 328, 628
Vink, J., & Laming, J. M. 2003, ApJ, 584, 758
Vink, J., Laming, J. M., Gu, M. F., Rasmussen, A., & Kaastra, J. S. 2003, ApJ, 587, L31
Westerlund, B. E. 1969, AJ, 74, 879
Whiteoak, J. B. Z., & Green, A. J. 1996, A&AS, 118, 329

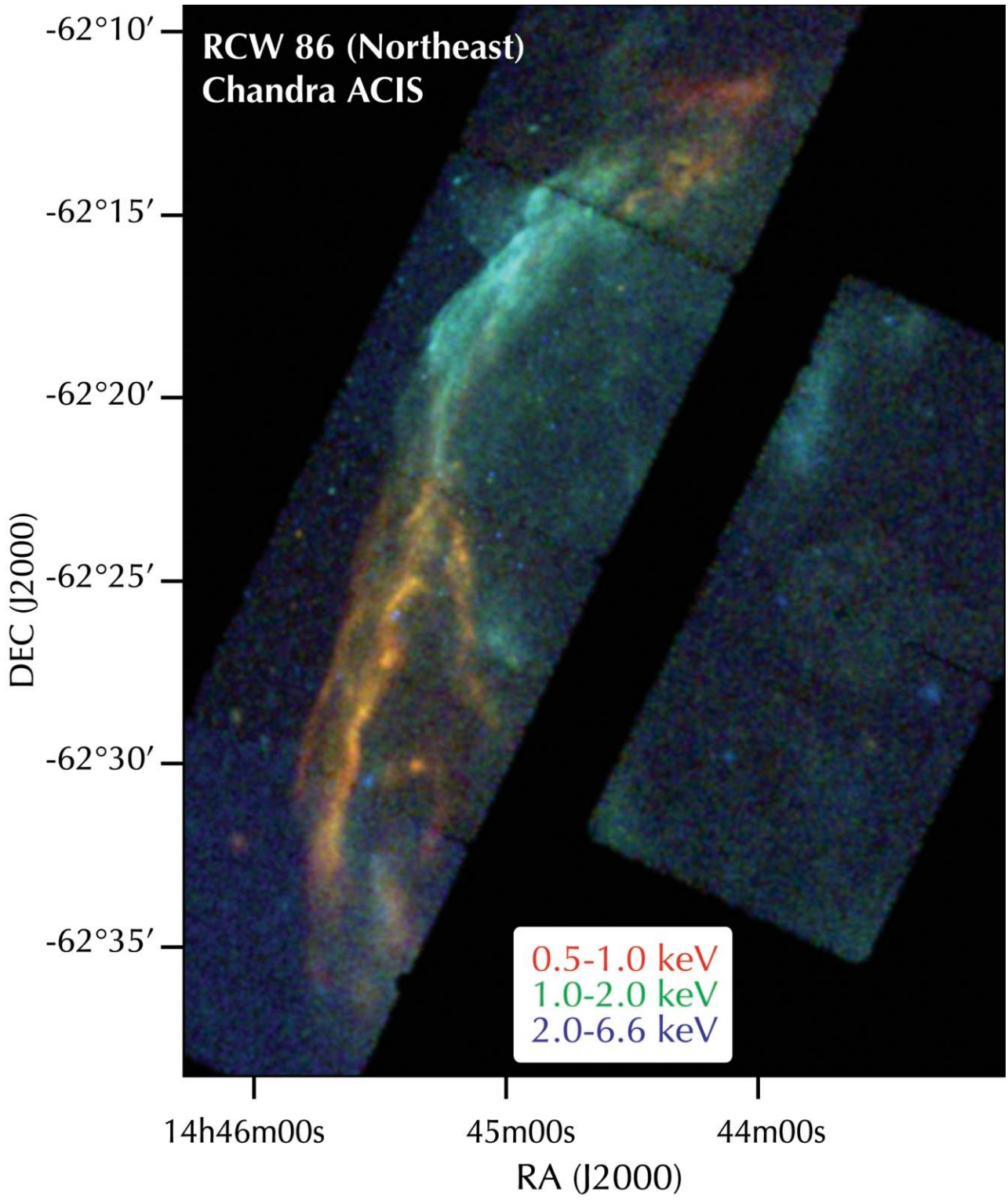

PLATE 1

FIG. 1.—*Chandra* exposure-corrected map of the northeastern part of RCW 86, using a square root brightness scaling. The red, green, and blue channels correspond to the 0.5–1, 1–1.95, and 1.95–6.6 keV energy bands, respectively.